J. COMBIN. MATH. COMBIN. COMPUT. 127b (2025) 5067--5088

Journal of Combinatorial Mathematics and Combinatorial Computing
www.combinatorialpress.com/jcmcc

Combinatorial Press

Dynamic modeling and quantitative computational assessment of grid power supply capacity at multi-temporal and spatial scales

Hujun Li[1], Yihan Zhang[1,✉], Man Jin[1], Xingwu Guo[1]

[1] *State Grid Henan Economic Research Institute, Zhengzhou, Henan, 450000, China*

ABSTRACT

Maximum supply capacity calculation is an important issue in grid planning, and with the large amount of renewable energy sources connected to the grid, the voltage instability problem becomes more and more prominent. In this paper, the maximum power supply capacity (TSC) of partitioned flexible interconnected grids under multi-temporal and spatial scales is dynamically modeled, and the TSC model is solved by using the deep deterministic policy gradient (DDPG) method to achieve quantitative assessment of the TSC of the grid. Meanwhile, the effectiveness of the model and algorithm is verified through simulation experiments. The stepwise approximation method and DDPG algorithm without considering the transient voltage stabilization constraints and the obtained TSC in which the node voltages are less than 0.80 p.u. are all greater than 1.0 s, and the transient voltages are destabilized. While the DDPG algorithm considering transient voltage stabilization, the obtained node voltage is greater than 0.80p.u., and the transient voltage is in a stable state, which indicates that the algorithm can effectively reduce the risk of transient voltage instability in the power grid. The sum of the TSCs of A and B divisions after the zonal flexible interconnection is 9348 MW, which is higher than the sum of the TSCs of 8696 MW during the zonal open-loop operation, indicating that the zonal flexible interconnection can improve the overall TSC level of the power grid. In addition, compared with the traditional algorithm and other reinforcement learning algorithms, the TSC calculation based on the DDPG algorithm is more efficient and accurate. This paper provides methodological guidance for evaluating the power supply capacity of power grids at multi-temporal and spatial scales.

Keywords: multi-temporal and spatial scales, maximum power supply capacity, zonal flexible interconnection, DDPG algorithm

✉ Corresponding author.
E-mail address: YihanHZhang@163.com (Y. Zhang).
Received 05 February 2024; Revised 12 April 2024; Accepted 05 December 2024; Published Online 16 April 2025.
DOI: 10.61091/jcmcc127b-282

1. Introduction

With the rapid development of industrialization and urbanization, the grid power industry plays a crucial role in modern society. As one of the very important infrastructures in modern industry and life, the power system plays an important role in realizing sustainable development and meeting the growing energy demand [1-4]. However, the power system faces a series of challenges in its actual operation, such as the imbalance between supply and demand, and therefore the assurance of power supply capacity plays a crucial role in the economic and social development of various fields [5-8].

Electricity supply capacity assurance is an important state of providing people with a reliable supply of electricity and ensuring the security and sustainability of the power supply, which plays an important role in the normal conduct of people's lives and the development of the country's economy [9-11]. The modern society has an increasing demand for electricity, both for household use and industrial production, which cannot be separated from a reliable power supply. The interruption of power supply may lead to a series of problems, such as transportation paralysis caused by power outage, medical equipment can not operate normally, etc., which brings great inconvenience to people's life and social order [12-15]. Therefore, power supply security is one of the core tasks of power grid construction and development. In order to guarantee the stability of power supply, grid operators have also taken a series of measures. Grid operators will carry out reasonable planning and design of the power grid to ensure the rational layout and sufficient capacity of the power supply network [16-19]. As for possible faults and accidents in the power grid, the grid operator finds and eliminates potential problems in time by establishing a sound monitoring system [20-21]. In addition, the grid operator improves the reliability and safety of the equipment through regular equipment overhaul and maintenance, and the implementation of these measures can effectively improve the reliability of power supply and ensure that people's life and production are carried out normally [22-23].

In this paper, for the problem of grid power supply capacity (TSC) calculation in multi-temporal and spatial scales, the construction and solution of TSC model for dynamic grid are realized with zoned flexible interconnection grid as the research object. First, the application background and working principle of zonal flexible interconnection are explained. Then, the TSC model of the zonal flexible interconnected grid is constructed, the TSC objective function, the equation constraints of AC and DC grids, and the constraints of N-1 static security constraints and transient voltage stability constraints are determined, and the DDPG algorithm is utilized to solve the TSC model. Finally, in order to verify the practicality of the model and algorithm, simulation experiments are designed to analyze the effects of transient voltage stability constraints, the capacity of partitioned interconnection devices, and the partitioned flexible interconnection method on the TSC of the grid, and the DDPG algorithm is compared with the traditional DE algorithm and other reinforcement learning algorithms.

2. Zonal flexible interconnected city grids at multiple spatial and temporal scales

2.1. Zonal flexible interconnection of urban grids

2.1.1. Operational status of the urban power grid. Power grid is an important infrastructure and strong guarantee for urban construction and development. With the construction of urban power grid, the scale of power grid is expanding, in order to make the short circuit capacity in the system does not exceed the circuit breaker's blocking capacity, and at the same time to avoid the formation of electromagnetic ring network, the traditional large-scale urban power grid is usually operated in a zoned and segmented way.

2.1.2. Partitioned flexible interconnection technology. Zonal flexible interconnection refers to the interconnection of urban power grid zones through flexible power electronic devices, through flexible power electronic devices to isolate the two ends of the zones, so that under the premise of not increasing the short-circuit current, can flexibly regulate the direction and size of inter-zonal current flow and appropriately compensate for the dynamic reactive power, to improve the security and stability of the urban power grid and power supply reliability.

In the case of grid zoning operation, in order to better adapt to the future situation, through the flexible interconnection technology for grid zoning contact is an effective strategy for future development. In this paper, we mainly investigate the dynamic modeling and quantitative calculation and evaluation of the maximum power supply capacity of the urban power grid when flexible interconnection technology is adopted in the case of power grid zoning.

2.1.3. Forms of zoned flexible interconnection wiring. At present, large urban power grid generally take 500kV ring network, 220kV zoning structure form, through the zoning flexible interconnection device on the urban power grid two or more zoning flexible interconnection, can realize the 500kV double-ring power supply, 220kV zoning interconnection of flexible closed-loop wiring form.

Sub-area flexible interconnection wiring schematic shown in Figure 1. City grid neighboring sub-districts usually exist between the contact line, in order to avoid the risk of excessive short-circuit current and electromagnetic ring network, under normal circumstances, the contact line is in a disconnected state. Under the form of zonal flexible interconnection connection, in order to save floor space, according to the internal and external space of the substation at both ends of the contact line, the zonal flexible interconnection device can be installed in the station at both ends of the contact line of the city grid zones (or in the adjacent area outside of the station), and priority is given to the use of the original standby contact line of the zones to contact the interconnected zones, so as to realize flexible interconnection of the city grid zones.

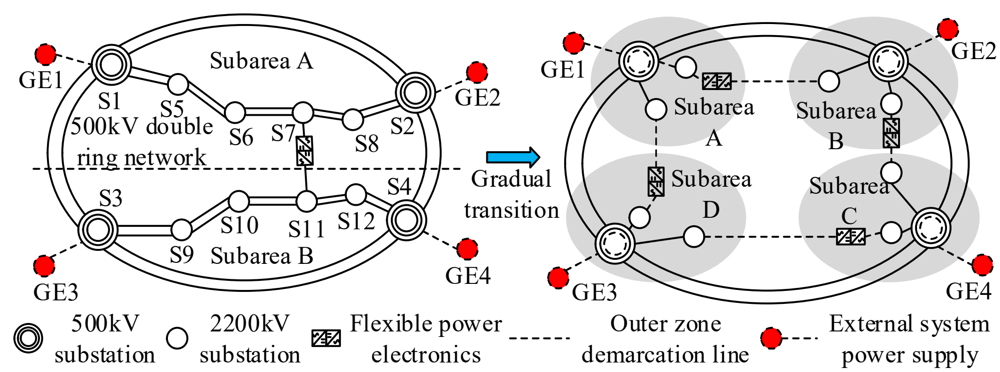

Fig. 1. Urban power grid zoning flexible interconnection connection form

Partition flexible interconnection wiring form, interconnection of the two partitions by flexible power electronic device isolation, can avoid a partition failure on the other partition of the impact, at the same time, the transmission power on the contact line can be controlled by flexible power electronic device. In addition, the flexible interconnection of the partition, the device and the partition of the connection point is equivalent to each increase a dynamic reactive power source, can enhance the power grid transient voltage stability.

2.2. Basic working principle of partition interconnectors

2.2.1. Basic structure of the device. The basic structure of the partitioned flexible interconnection device is shown in Figure 2. The partitioned interconnection device consists of 2 symmetrical MMCs, which are illustrated with MMC_1 end parameters as an example. The AC grid parameters are: U_{s1}

is the fundamental frequency voltage of bus 1. P_{s1} is the value of active power exchange between bus 1 and the device. Q_{s1} is the reactive power exchange value of bus 1 with the device. X_{trl} is the equivalent reactance of the coupling transformer. The internal parameters of the device are: U_{c1} is the base frequency voltage output from the device. U_{dc} is the internal DC voltage of the device, which is usually kept constant. I_{dc} is the internal DC current of the device. R_1 is the equivalent resistance of the MMC_1 losses. X_{L1} is the equivalent reactance of the MMC_1 valve reactor.

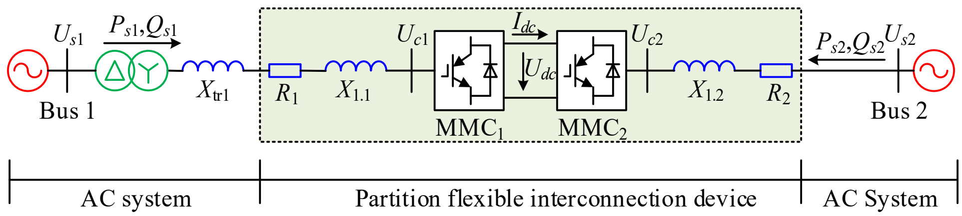

Fig. 2. Structure of partition flexible interconnection device

2.2.2. Mode of operation of the device. The regulation of active and reactive power of zonal flexible interconnection device can improve the current distribution and voltage situation of urban power grid. Based on the characteristics of flexible interconnection in different states of power grid, the following three operation modes of the device are proposed from the perspective of power grid planning and operation.

Mode 1: Load balancing mode

Under normal operation, the zonal flexible interconnection device controls the flow of active power from light-loaded zones to heavy-loaded zones according to the load levels of the two zones under the premise of maintaining the emergency support capacity in order to balance the load conditions of the two zones and optimize the current distribution.

Mode 2: Emergency active support mode

When a sub-district is overloaded due to a power shortage caused by a grid fault or maintenance, the device controls active power from another sub-district to provide emergency support to that sub-district to eliminate the overload problem.

Mode 3: Dynamic reactive power support mode

When there is a risk of voltage instability in a partition, the device urgently provides dynamic reactive power to support the voltage, avoiding voltage instability and achieving the purpose of improving transient voltage stability.

Mode 1 is the normal state, and modes 2 and 3 are the emergency state. The main purpose of the zonal flexible interconnection device is to function in the emergency state, and it can also cooperate with other regulation measures to participate in the optimization of the voltage reactive power during normal operation under the premise of maintaining sufficient residual capacity.

2.2.3. Principle of device current control:

1) Selection of control mode of the device. The zonal flexible interconnection device adopts a direct current control strategy based on the synchronous rotating coordinate system to realize active and reactive power decoupling control. Among them, the MMC at any $i(i=1,2)$ end can choose the following 4 control methods:

(1) Fixed AC active power P_{si} and reactive power Q_{si} control.

(2) Constant AC active power P_{si}, bus voltage U_{si} control.

(3) Constant DC voltage U_{dc}, AC reactive power Q_{si} control.

(4) Constant DC voltage U_{dc}, AC bus voltage U_{si} control.

In order to maintain the active balance between the two ends of the device, it is necessary to select one end of the MMC to control the DC voltage and act as a balancing station, and the other end to control the active current. Therefore, four combinations of control modes can be selected at both ends of the device: a and c, a and d, b and c, b and d.

For the load balancing mode and emergency active support mode, the device mainly regulates the active current between sub-divisions and uses the remaining capacity to provide reactive power compensation to optimize the grid current. In order to facilitate the control of the power transfer value, the device is set to adopt a combination of control modes a and c for these two modes of operation. For the dynamic reactive power support mode, to stabilize the node voltage, the device selects a combination of control methods b and d. The above control modes are uniformly controlled at the system level, and can be controlled at the ms level.

2) Power transfer equation of the device. Taking the MMC_1 end of the device as an example, the equivalent phase change reactance is:

$$X_1 = X_{tr1} + X_{L1} \tag{1}$$

Since R_1 is small and usually ignored in the analysis, there is:

$$P_{s1} = \frac{kU_{s1}U_{c1}\sin\delta_1}{X_1} \tag{2}$$

$$Q_{s1} = \frac{kU_{s1}\left(U_{c1}\cos\delta_1 - kU_{s1}\right)}{X_1} \tag{3}$$

where k is the coupled variable ratio, δ_1 is the phase angle difference between U_{s1} and U_{c1}.

There exists a relationship between U_{c1} and DC voltage U_{dc} as shown in equation (4):

$$U_{c1} = \frac{\sqrt{6}}{4}M_1U_{dc} \tag{4}$$

where M_1 is the device voltage modulation ratio.

3) Capacity constraints of the device. In actual operation, the active P_{s1} and reactive Q_{s1} power transmitted by the device is limited by the capacity S_r of the device:

$$P_{s1}^2 + Q_{s1}^2 \le S_r^2 \tag{5}$$

2.2.4. Determination of the dynamic reactive power output range of the device. From equation (5), the active power P_{s1} transferred by the device and the reactive power compensation Q_{s1} provided need to satisfy the device capacity constraint.

From Eq. (2) and Eq. (3):

$$P_{s1}^2 + \left[Q_{s1} + \frac{\left(kU_{s1}\right)^2}{X_1}\right]^2 = \left(\frac{kU_{s1}U_{c1}}{X_1}\right)^2 \tag{6}$$

From equation (4), U_{c1} is related to the modulation ratio M_1. Setting M_{max} and M_{min} as the maximum and minimum values of the modulation ratio, respectively, the maximum and minimum values of U_{c1} can be obtained by substituting U_{cmax} and U_{cmin} into Eq. (6) to obtain the constraints of the device in operation as shown in Eqs. (7) to (8):

$$P_{s1}^2 + \left[Q_{s1} + \frac{\left(kU_{s1}\right)^2}{X_1}\right]^2 „ \left(\frac{kU_{s1}U_{cmax}}{X_1}\right)^2 \tag{7}$$

$$P_{s1}^2 + \left[Q_{s1} + \frac{(kU_{s1})^2}{X_1} \right]^2 \geq \left(\frac{kU_{s1}U_{c\min}}{X_1} \right)^2 \tag{8}$$

From Eq. (5), Eq. (7) and Eq. (8), the power output range on the device MMC_1 side can be plotted as shown in Fig. 3. The area enclosed by the solid line in the figure is the power output range, and the upper horizontal axis indicates the output reactive power and the lower one indicates the absorbed reactive power.

Due to the limitation of the range of modulation ratios, the maximum reactive power output of the device (corresponding to point A) may be less than the capacity of the device (corresponding to point C) at a certain value of ratio k of the connected transformer. It is possible to change the range of reactive power output by adjusting k, but during the transient process after $N-1$, the transformer tap cannot be actuated quickly enough, so the maximum dynamic reactive power compensation that can be output is actually the reactive power value corresponding to point A.

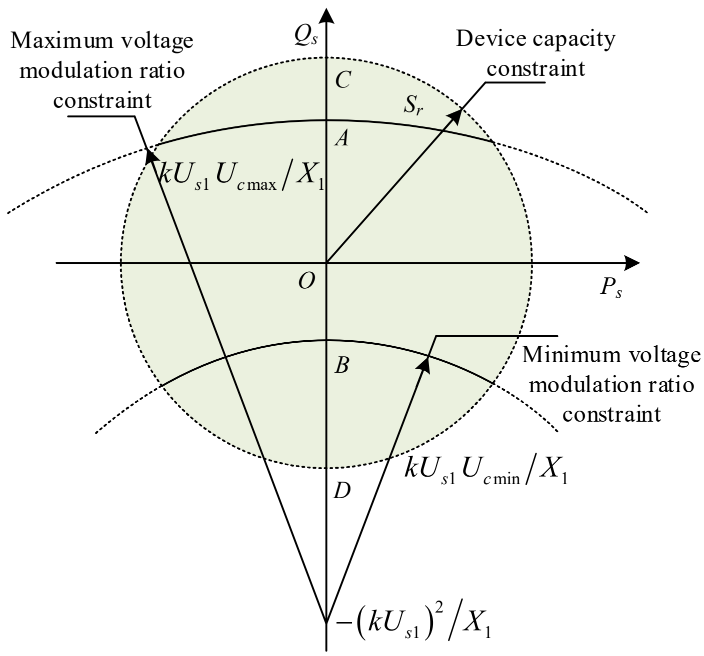

Fig 3. MMC1-side power output range of device

3. Quantitative assessment model of the maximum capacity of a zonal flexible interconnected grid

3.1. TSC model for zoned flexible interconnected urban grids

3.1.1. TSC for zoned flexible interconnected grids. The maximum power supply capacity (TSC) of a distribution network refers to the maximum load that can be supplied by the grid in a certain power supply area based on certain boundary constraints, which is an important indicator reflecting the security and efficiency of the distribution system. And the calculation of TSC of zonal flexible interconnected urban grids needs to consider the following 2 points:

1) The security of all partitions needs to be taken into account at the same time.

2) The active support and dynamic reactive power support of zonal interconnection devices should be considered, and the devices can equalize zonal loads during normal times and stabilize the grid voltage during the transient process after a fault.

Therefore, this paper defines the zonal flexible interconnected grid TSC as the maximum available load of the grid that meets the overall N-1 static security and transient voltage stability constraints for a certain output state of power plants in the region, taking into account the active support and dynamic reactive power support of interconnection devices.

3.1.2. TSC objective function. Assuming that Partition A is flexibly interconnected with Partition B through an interconnection device, the two partitions become a whole and the objective function of the grid TSC is:

$$f_{TSCA+B} = \max \sum_{i \in (\hat{A}+B)} P_{Li} \tag{9}$$

Where, f_{TSCA+B} denotes the TSC of partition A & B as a whole. $i \in (A+B)$ denotes the node i is the node of partition A & B. P_{Li} is the active load of node i.

3.1.3. Model Equation Constraints:

1) AC grid equation constraints. The AC grid equation constraint is the tidal equation constraint. When a node in the grid is not connected to a device, the tidal equation does not need to be changed. When the nodes are connected to the device, the power transferred between the grid and the device needs to be accounted for. Assuming that the device absorbs active and reactive power from the AC grid, the tidal equation is modified to:

$$\begin{cases} P_i - U_i \sum_{j \in i} U_j \left(G_{ij}^s \cos\theta_{ij} + B_{ij}^s \sin\theta_{ij} \right) - P_{si} = 0 \\ Q_i - U_i \sum_{j \in i} U_j \left(G_{ij}^s \sin\theta_{ij} - B_{ij}^s \cos\theta_{ij} \right) - Q_{si} = 0 \end{cases} s \in \Omega \tag{10}$$

Where, P_i, Q_i are the active and reactive power injection values of the node i connected to the device, respectively. P_{si}, Q_{si} are the active and reactive power values absorbed by the device from node i, respectively. $j \in i$ indicates that node j is the node associated with node i. U_i, U_j are the node i, j voltage magnitude respectively. Ω is the grid $N-1$ fault set. G_{ij}^i and B_{ij} are the grid conductance and conductance parameters for the Sth fault case, respectively. θ_{ij} is the phase angle difference of node i and j voltages.

where P_i, Q_i are shown in equation (11):

$$\begin{cases} P_i = P_{Gi} - P_{Li} \\ Q_i = Q_{Gi} - Q_{Li} \end{cases} \tag{11}$$

Where, P_G and Q_{Gi} are the active, reactive power injections of the generator at node i, respectively. $P_{L,i}$ and $Q_{L,i}$ are the active, reactive loads of node i, respectively.

In the actual power grid, the load changes of different load points in a region are generally proportional, i.e., the load at each node satisfies equation (12):

$$P_{Li} = P_{L0i} + \lambda b_{pi} \tag{12}$$

Where, $P_{L,0i}$ is the initial load, λ is the load growth parameter and b_{pi} is the direction of load growth. Assume Q_L varies with P_{Li} according to the constant power factor.

2) DC device equation constraints. The DC device should satisfy the equation constraints of Eqs. (1) to (4). In addition, since the active loss R of the MMC is negligible, the active power P_{si} flowing into MMC_i should be balanced with the DC power, denoted as:

$$P_{si} = U_{dc} I_{dc} \tag{13}$$

3.1.4. Model inequality constraints:

1) $N-1$ Static security constraints. The grid needs to satisfy $N-1$ static security requirements, including main transformer capacity constraints, line capacity constraints & node voltage constraints, denoted as:

$$\begin{cases} T_i^s \le T_i^{\max} \\ R_{Fij}^s \le R_{Fij}^{\max} \\ U_i^{\min} \le U_i^i \le U_i^{\max} \end{cases} \quad s \in \Omega \tag{14}$$

Where, T_i^s, R_{Fij}^s and U_i^s are the main transformer load, line load and node voltage after the sth $N-1$ faults respectively. The superscripts min and max on the variables indicate the lower and upper values of the variables, respectively.

The DC device should satisfy not only the capacity constraint Eq. (5) but also the device voltage modulation ratio constraint:

$$M_i^{\min} \le M_i \le M_i^{\max} i = 1,2 \tag{15}$$

2) Transient voltage stability constraints. During the transient process of $N-1$ faults occurring in the power grid, the voltage stability needs to be calibrated to ensure that the transient voltage security of the power grid will not be affected after the load growth.

The power system transient voltage stability is in accordance with the following criteria:

$$U_i^s \left(t_c + t_{\lim} \right) \ge U_{\lim} \ s \in \Omega \tag{16}$$

Where, t_c is the fault clearing time. Time after fault clearance $t_{\lim} = 10s$. Load bus voltage $U_{\lim} = 0.8 p.u.$.

When the system returns to steady state, each bus voltage cannot be higher than the set upper limit of steady state voltage to prevent overvoltage at the system buses, which can be expressed as:

$$U_i \left(t_c + t_{cl} \right) \le U_i^{\max} \tag{17}$$

where t_d is the time for the system to return to steady state after the fault is cleared.

In addition, during the fault transient process, the device needs to satisfy the constraints shown in Eq. (5), Eq. (7) & Eq. (8), and the maximum dynamic reactive power compensation value that can be provided should be less than the maximum reactive power output value in actual operation.

3.2. DDPG-based model solving methods

In this paper, the DDPG algorithm is used to calculate the TSC of the zonal flexible interconnected grid to ensure the power supply capacity while reducing the risk of future dynamic voltage instability in the grid.

3.2.1. Deep Deterministic Policy Gradient Method (DDPG). Deep Deterministic Policy Gradient (DDPG) [24] was developed from Deep Q Learning (DQN) [25]. The difference between DDPG and DQN is that DDPG describes continuous actions, while DQN describes discrete actions. For DQN, the result of the output of the environmental action and strategy network is the score of different actions, and then the model may choose a large one based on the probability. But for DDPG, the final output is directly the action values. Also, they use different strategy networks, DQN uses a classification function like softmax, while DDPG uses a continuous value function like tanh.

First the max function formula is:

$$\begin{cases} a, if\ a \geq b \\ b, if\ a < b \end{cases} \tag{18}$$

The difference between the softmax function and max is that it is hoped that the item with a large score is often taken, rather than only the large score can be taken, softmax function can be used to calculate the probability of a and b taken, the probability of being taken is related to their size. tanh function formula:

$$f(z) = \frac{e^{z} - e^{-z}}{e^{z} + e^{-z}} \tag{19}$$

Deep Deterministic Policy Gradient (DDPG) is a method that uses a neural network to compute the state to get the selected action, executes the action to get the new state and reward, and then puts the samples into the experience playback pool for neural network training.The basic algorithmic implementation framework of the DDPG algorithm is shown in Fig. 4. It does not require model inputs and can handle high dimensional spaces quickly. The deterministic strategy is compared with the stochastic strategy. For some action sets, it may be continuous values or high-dimensional discrete values, so the spatial dimensions of the actions are large. In this case, matrix processing works better.

The Actor-Critic framework used in DDPG is a process of iterative training of the strategy network and the Q-network through the interaction of the environment, the Actor network and the Critic network in the context of a cyclic plot and time step. The empirical pool, the dual Actor network and the dual Critic network are the three important components of the DDPG. The role of the Critic network is to predict the Q, with inputs such as actions and states. The function of the Actor network is to output an action A, which is input to the Critic to maximize the value of the Q. The Actor update is influenced by the Critic network, using a the gradient ascent method. The empirical pool is used because the transformed data sequences obtained when the Actor network interacts with the environment are highly temporal. If these data sequences were used directly for training, the neural network would overfit and not converge easily. Therefore, it is necessary to disrupt the temporal sequence, and the Actor network in this framework first stores the transformed data into the storage space, and then randomly extracts a small batch of data from the storage space during the training process, so that the extracted data can be treated as time-independent data.

The parameters of the target network in DDPG iteratively approximate the parameters of the main network by a tiny amount each time. The network parameters are updated specifically: the Critic network gradient update parameters for the current network, the Critic network soft update parameters for the target network, the Actor network gradient update parameters for the current network, and the Actor network soft update parameters for the target network.

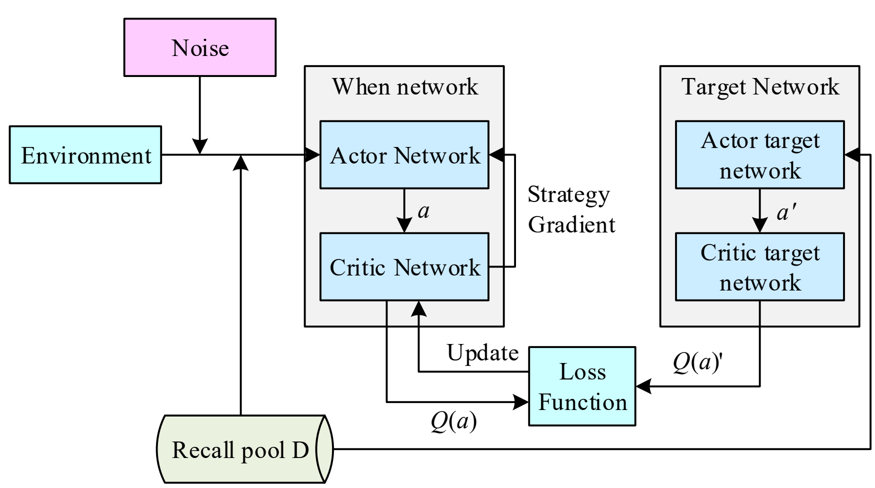

Fig. 4. Flowchart of DDPG algorithm

3.2.2. Specific steps of the DDPG algorithm. The specific steps of the DDPG algorithm are as follows:

Firstly, the input parameters: Actor current network, Actor target network, Critic current network, Critic target network, their parameters θ, θ', w, w'. decay factor γ, soft update coefficient τ, number of samples for batch gradient descent m, target Q frequency of updating the network parameters C. Maximum number of iterations T. Randomized noise function. Where the noise function selects Gaussian noise as in equation (20):

$$Noise(x)=\frac{1}{\sqrt{2\pi}\delta}e^{\frac{-(x-\mu)}{2\delta^2}} \tag{20}$$

Output: optimized parameters, Actor's current network parameter θ, Critic's current network parameter w. And the action values obtained from the optimization.

1) Randomly initialize θ, θ', w, w', where $\theta=\theta'$, $w=w'$. Reset the set of reminiscence pools for placing experience replay D.

2) Start the iteration: Step1: Initialize the first state S.

Step2: Calculate the action A when we get state S using Actor network. Where A is calculated as follows:

$$A=\pi_\theta(\phi(S))+Noise \tag{21}$$

Step3: Perform action A to get new state S'.

Step4: Pass $\{obs, action, reward, next\_obs, done\}$ into the experience pool D. where obs is the state, $action$ is the action, $reward$ is the rating under that state and action, $next\_obs$ is the next state, and $done$ is whether or not the model ends. In this study, $done$ reaches the end of the computation cycle with a value of $True$ and all others are $False$.

Step5: Update the state, $S=S'$.

Step6: Play back m samples from the experience pool and calculate the current Q value:

$$y_j=\begin{cases} Rj & doneistrue \\ Rj+\gamma Q'\left(\phi\left(S_j'\right),\pi_{\theta'}\left(\phi\left(S_j'\right)\right),w'\right) & doneisfalse \end{cases} \tag{22}$$

Step7: The gradient of parameter w of the Critic network is updated using the mean square error loss function, where the formula for the mean square error loss function is:

$$J(w)=\frac{1}{m}\sum_{j=1}^{m}\left(y_j-Q\left(\varnothing\left(s_j\right),A_j,w\right)\right)^2 \tag{23}$$

Step8: Update the parameter θ of the Actor network. the Actor wants to get as big a Q value as possible, so the Actor network can simply be interpreted as the larger the value of the feedback Q the smaller the loss, the smaller the value of the feedback Q the larger the loss, so the Actor's loss function simply puts a minus sign on the value of Q returned by the state estimation network:

$$J(\theta)=-\frac{1}{m}\sum_{i=1}^{m}Q\left(S_i,A_i,\theta\right) \tag{24}$$

Step9: When the parameter update condition is reached, update the parameters of Critic target network and Actor target network:

$$\begin{cases} w'=\tau w+(1-\tau)w' \\ \theta'=\tau\theta+(1-\tau)\theta' \end{cases} \tag{25}$$

Step10: If $done$ is $True$, end the loop. Otherwise, go to Step2.

4. Simulation analysis

4.1. Simulation parameters

In order to verify the effectiveness of the DDPG algorithm in solving TSC, this paper performs TSC calculations for two partitions, A and B, of a 220kV partitioned flexible interconnected grid. The two partitions contain 61 nodes, 51 load nodes, 5 power plant nodes, 5 500kV nodes and 56 220kV nodes. The Flexible DC Interconnection Device (FDCID) is located between nodes 27 and 39 and has a capacity of 900 MVA. The geographical wiring of the grid is shown in Fig. 5.

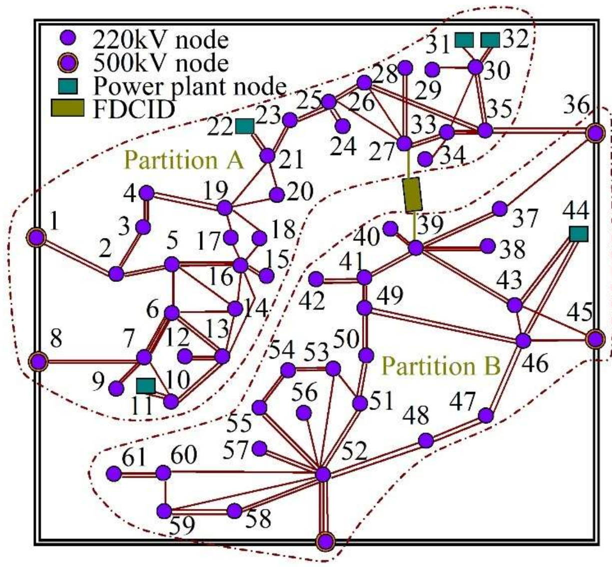

Fig. 5. System geographic connection diagram

The design DDPG training parameters are shown in Table 1, and the values of the algorithm parameters are obtained through experiments so that the algorithm has good performance in solving TSC.

Table 1. Training parameters of DDPG algorithm

Training parameters	Parameter Value
Number of iterations	12000
Actor network learning rate	1×10^{-3}
Critic network learning rate	1×10^{-4}
Discount factor γ	0.9
Experience playback set size	1×10^{6}
Sample set size	122
Renewal coefficient	1×10^{-3}

4.2. Effect of transient voltage stabilization constraints on TSC calculation results

The models and algorithms in this paper are applied to solve the TSC of the above grid, and the models without considering the transient voltage stabilization constraints are solved by the stepwise approximation method and the DDPG algorithm, respectively, and the comparisons of the TSC results of different models and algorithms are shown in Table 2.

The TSC results obtained by the DDPG algorithm are better than those of the stepwise approximation method, and the TSC decreases slightly after considering the transient voltage stabilization constraints, which are analyzed as follows:

1) The power of each load point in the stepwise approximation method grows according to the synchronization length. The calculated TSC is not optimal. And the power of each node in DDPG varies according to different step lengths, which is more suitable for reality.

2) If a voltage instability occurs at a node in the grid and a flexible interconnection device is needed to provide power support, the TSC considering the transient voltage stabilization constraints will decrease slightly due to the capacity limitation of the device.

Table 2. Training parameters of DDPG algorithm

TSC calculation methods and constraints	TSC/MW
Step by step approach method without considering transient voltage stability	9435
DDPG algorithm without considering transient voltage stability	9502
DDPG algorithm considering transient voltage stability	9348

Under the disturbance of 60MW sudden load increase, to verify whether the voltage instability occurs in the TSC calculated by different constraints and algorithms, the transient voltage stabilization criterion is designed by using the time-domain simulation method: if the node voltage is lower than 0.8 p.u. for a duration of less than 0.8s after the fault is cleared for 10s, then it is stable, if it lasts for 0.8-1.0s, then it is critically stable, and if it lasts for more than 1.0s, then it is unstable. From the above grid data node 54 has the maximum load factor and hence node 54 is analyzed. The voltage profile of node 54 solved by different models and algorithms is shown in Fig. 6. Where, Algorithm 1, Algorithm 2, and Algorithm 3 denote the stepwise approximation method without considering transient voltage stabilization, the DDPG algorithm without considering transient voltage stabilization, and the DDPG algorithm considering transient voltage stabilization, respectively.

From Fig. 6, it can be seen that in the stepwise approximation method without considering transient voltage stabilization constraints and the DDPG algorithm and the obtained TSC, node 54 has a voltage less than 0.80 p.u. on time periods 0.31-3.72s and 0.31-7.05s, respectively, which are both greater than 1.0s, and the transient voltage is destabilized. While the DDPG algorithm considering transient voltage stabilization, the obtained voltage of node 54 is greater than 0.80 p.u. Therefore, considering transient voltage stabilization can effectively reduce the risk of transient voltage destabilization of the power grid.

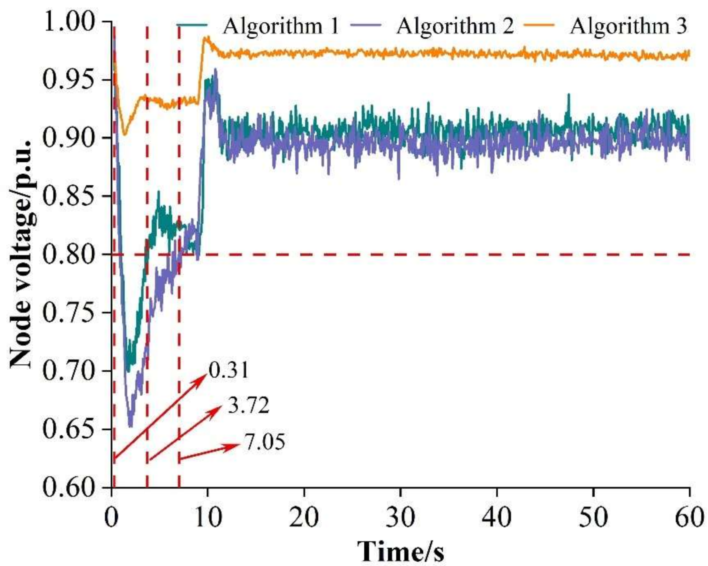

Figure 6. Voltage curves of node 54 solved by different models and algorithms

4.3. Impact of Zoned Flexible Interconnect Unit Capacity on TSCs

In order to study the effect of different capacities of flexible interconnectors on TSC, this paper calculates the TSC of different capacities for the above grid as shown in Fig. 7. Among them, TSC1 and TSC2 denote the TSC models without considering transient voltage stabilization and considering transient voltage stabilization, respectively.

As the capacity of the zonal flexible interconnectors increases, the TSC of the grid is significantly increased and the TSC is reduced by the dynamic voltage stabilization constraints for the same capacity. However, when the capacity exceeds 900 MW, the TSC increase is not significant, the configuration cost is higher, and the decrease in TSC affects the economy.

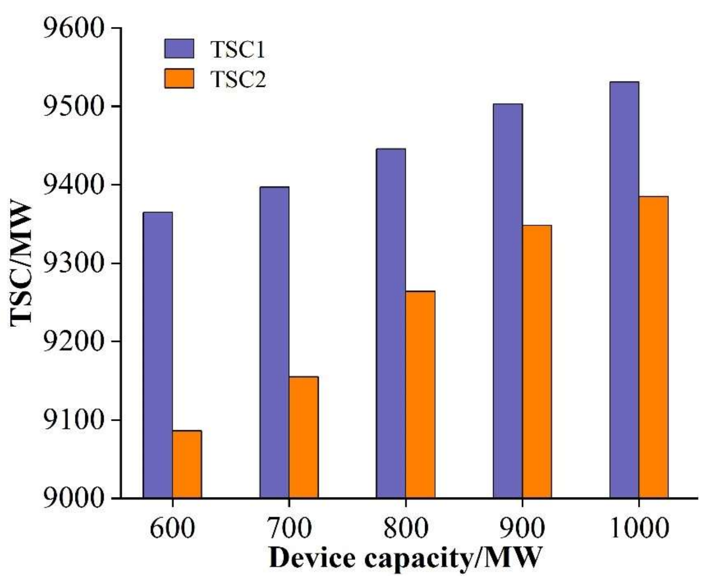

Fig. 7. Influence of different capacity of interconnect device on TSC

4.4. TSC calculation results and analysis

In order to verify the superiority of the zonal flexible interconnection technique used in the grid, this section compares it with the zonal open-loop operation and calculates the TSC of the grid using the DDPG algorithm, respectively.

4.4.1. Calculation of initial parameters. The zonal flexible interconnection grid in Fig. 5 is used as an example to verify the correctness and practicality of the model and algorithm in this paper. The voltage modulation ratio of the partitioned interconnection device $M_{max} = 0.95$, $M_{min} = 0.95$.

When the grid partitioned open-loop operation, TSC should be calculated separately for the two partitions individually, and node i in the objective function of Eq. (9) is only taken as the node of a certain partition, and the part of the device in the constraints is removed.

Set the initial load change step $\lambda = 0.1$ and the convergence accuracy $\varepsilon = 0.001$. The upper and lower limits of bus voltage in the N-1 static security analysis are set to 1.05 p.u. and 0.9 p.u., respectively. The N-1 fault set is selected as follows:
1) A main transformer within the 500kV node of the sub-division is removed due to a fault.
2) A single 500kV double circuit line in the sub-district is removed due to fault.
3) A single circuit of the 220kV double circuit in the sub-district is removed due to a fault.

The static security analysis shows that at this load level, there is a situation in which the N-1 calibration of the grid cannot be passed, so the load carried by each node when the grid reaches the TSC should be lower than this load level, and in the process of approximating the calculation of the TSC, the load of each node is scaled down proportionally.

In order to analyze the convenience, set the partition interconnection device directly connected to the grid at both ends, at this time the device can provide dynamic reactive power compensation that is the capacity of the device 900MVA. simulation process using two STATCOM to equate the device's dynamic reactive power compensation role. The transient simulation parameters of the device are shown in Table 3.

Table 3. Transient simulation parameters of partition interconnection devices

Device parameters	Parameter value
The time constant of the filter and the measurement loop /s	0.02
Proportional link time constant /s	0.02
Device response delay /s	0.01
Proportional link magnification	10
Integration link magnification	50
Device V-I characteristic curve slope	0.02
Upper limit of voltage limiting link /p.u.	1.0
Lower limit of voltage limiting link /p.u.	-1.0
Maximum capacitive current /p.u.	1.0
Maximum inductive current /p.u.	1.0

4.4.2. TSC calculations under open-loop operation:

1) TSC calculation result of partition A. After calculation and simulation analysis, it can be obtained that the TSC calculation result of sub-district A is 4366 MW when the sub-district is open-loop operation, and the limitation of TSC is due to the destabilization of the sub-district voltage after the main transformer N-1 in node 22 in sub-district A. Taking the 220kV bus at node 28 as an example, the voltage recovery after N-1 of the main transformer within node 22 is shown in Fig. 8. It can be seen that the 220kV bus at node 28 cannot recover to more than 0.8 p.u. within 10s and the voltage is destabilized.

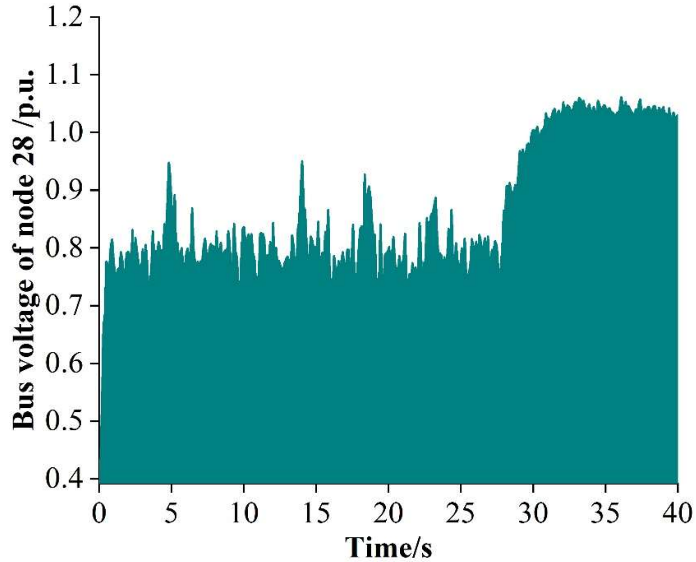

Fig. 8. Bus voltage of node 28 behind N-1 at node 22 during partition open loop running

2) Calculation results of TSC in partition B. After calculation and simulation analysis, it can be obtained that the result of TSC calculation for partition B is 4330 MW when the partition is open-loop operation, and the limitation of TSC is due to the destabilization of the partition voltage after the main transformer N-1 in node 44 in the B partition. Taking the 220kV bus at node 46 as an example, the voltage recovery of this bus after the main transformer within node 44 is removed with N-1 fault is shown in Fig. 9. The 220kV bus at node 46 is similarly unable to recover above 0.8 p.u. within 10s and the voltage is destabilized.

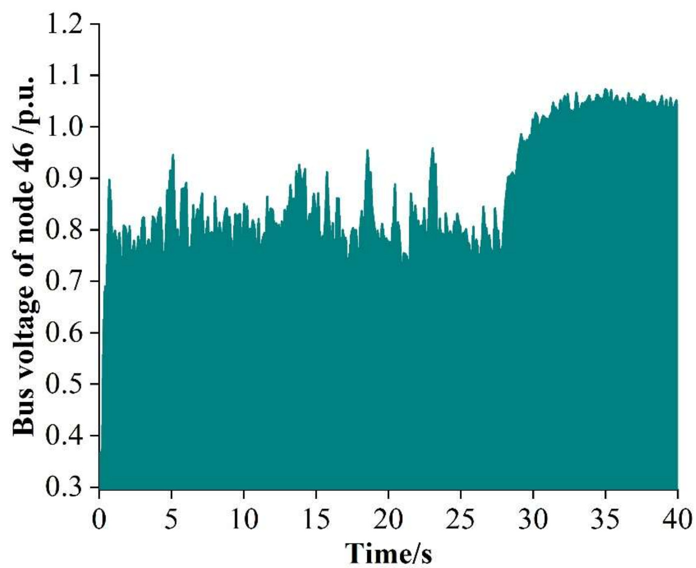

Fig. 9. Bus voltage of node 46 behind N-1 at node 44 during partition open loop running

4.4.3. TSC Calculations at Partitioned Flexible Interconnections. The contact line between partition A and partition B is connected with a partition interconnection device, at which time the two partitions become a whole, and the TSC value of the whole grid should be calculated. After simulation analysis, the TSC level of the whole network after the partition flexible interconnection is 9348 MW, and at this time, the partition interconnection device controls the active support of 188 MW from partition B to partition A. The limitation of the TSC is due to the fact that the remaining lines are fully loaded after the N-1 fault of a single line in node 21 - node 22 double-loop line, and at this time, the transient voltage of the grid is stable, and still taking the 220 kV bus at node 46 as an example, the voltage recovery of the main transformer in node 44 after N-1 is stable, and the voltage recovery of node 44 after N-1 is not stable. 44 within the main transformer after N-1 voltage recovery is shown in Fig. 10. In this case, the reactive output of the converter on the coupling side of the unit with node 39 is shown in Fig. 11. It can be seen that the 220kV bus voltage at node 46 reaches a stabilized value of 1.07 p.u. in 0.8s. The device quickly provides dynamic reactive power compensation after a grid fault, and the reactive power compensation reaches a maximum of 900MVA in 0.5s, which improves the transient voltage stability of the grid.

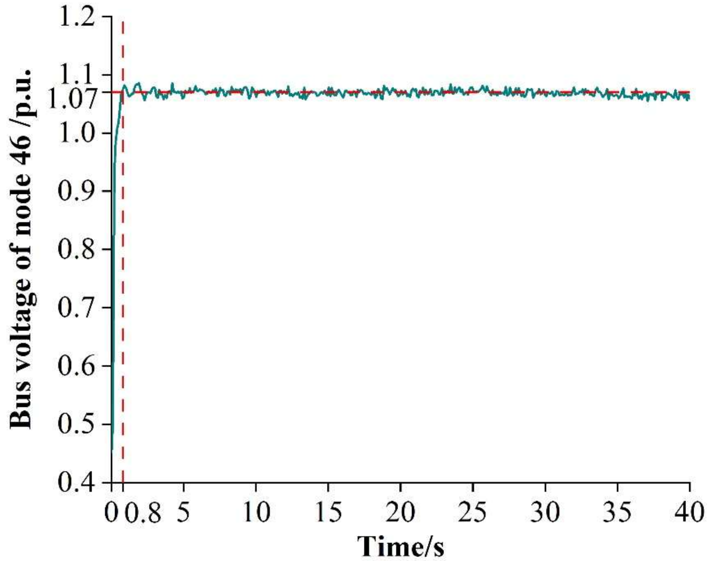

Fig. 10. Bus voltage of node 46 during the zoned flexible interconnection

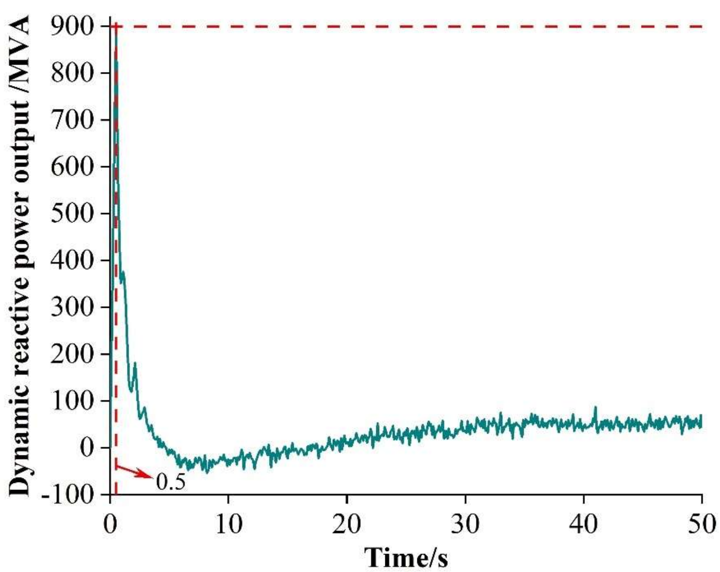

Fig. 11. Dynamic reactive power output of the node 39 partition interconnection device

From the above TSC calculations, it can be seen that the method in this paper considers both N-1 static security constraints and transient voltage stabilization constraints, which is in line with the practical requirements for security of large-scale power grids at multi-temporal scales. After the partitioned flexible interconnection, both the active support role of the interconnected devices and the dynamic reactive power support role of the devices are considered, and the results obtained are reasonable. During the open-loop operation, the TSCs of subarea A and subarea B are 4366 MW and 4330 MW, respectively, and the sum of the TSCs of the two subareas is 8696 MW, whereas the sum of the TSCs of the two subareas after the flexible interconnection of the two subareas is 9348 MW, which can be seen that the overall TSC level of the grid is improved after the flexible interconnection of the subareas. Further analyzing the reason for limiting TSC, it can be seen that in the case of open-loop operation, the dynamic reactive power in the area is insufficient, and the TSC is limited by the transient voltage stability. After the zonal flexible interconnection, a STATCOM is added at both ends of the device for two zones, which can improve the voltage stability. Therefore, the overall load carried by the grid can continue to increase.

4.5. Comparative analysis of TSC calculation results for different solution algorithms

4.5.1. TSC calculation based on DDPG algorithm. The curves of the loss function and the reward value function with the number of training times computed by the DDPG algorithm are shown in Fig. 12, respectively (a and b are the loss function and reward value, respectively). The loss function and reward value start to converge around 3200 times of training and the optimal solution is obtained at 3820 times.

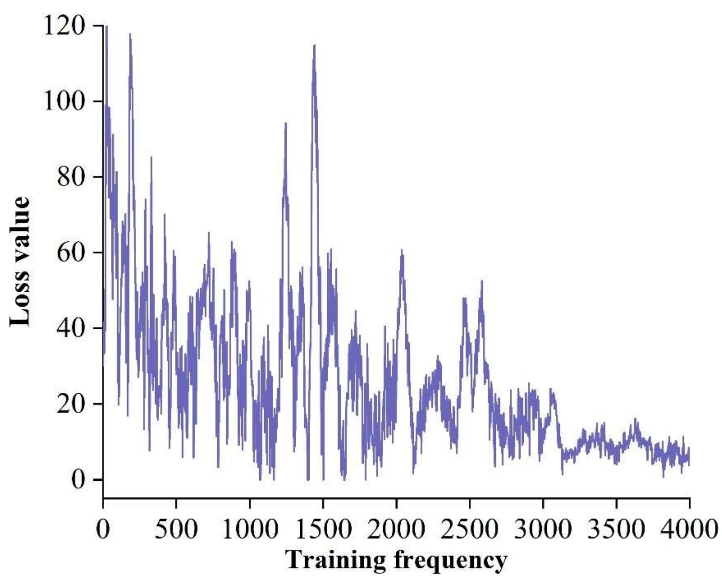

(a) Loss function

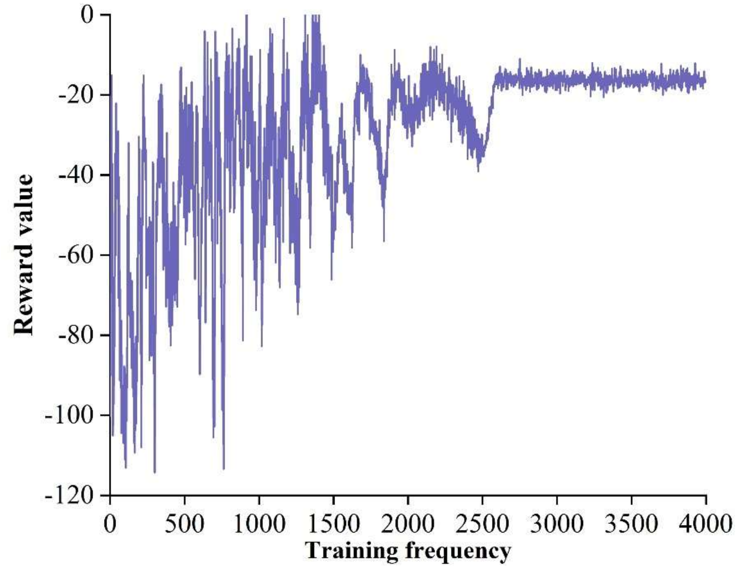

(b) Reward value

Fig. 12. Variation curve of loss function and reward value

The curve of the TSC of the grid with the number of training times is shown in Fig. 13. And the TSC of the grid starts to converge to a fixed value of 9348 MVA around 3500 times of training, indicating that the computation reaches the optimization.

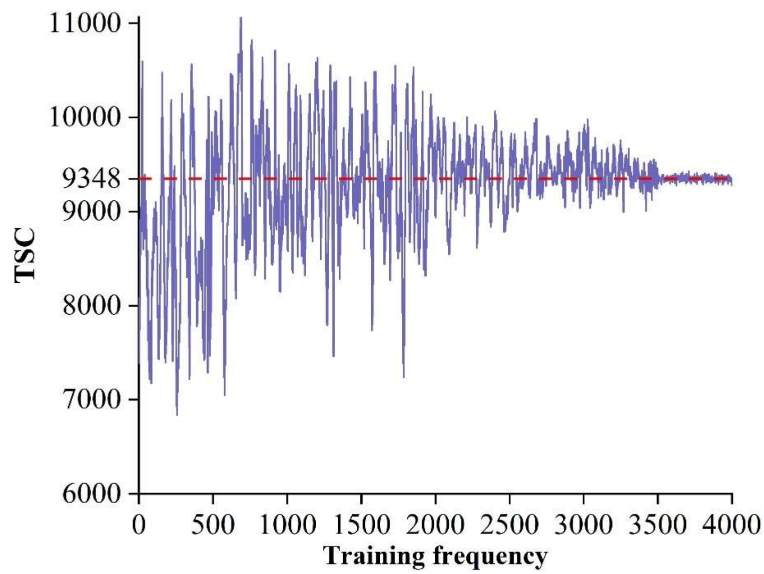

Fig. 13. TSC curve of power grid with training times

4.5.2. Comparison with traditional TSC calculation methods. The traditional DE algorithm [26] is applied to simulate this paper's algorithm, and the comparison results with this paper's DDPG algorithm are shown in Table 4.

From Table 4, it can be seen that the number of calculations of DE is relatively high, which is due to the fact that DE cannot utilize the prior knowledge of individuals in the later stage, the variability between individuals decreases, the convergence speed is slow, and the number of iterations increases, whereas DDPG can utilize the previous learning experience, which improves the speed of calculations. The TSC value obtained by DE is the smallest, which is due to the fact that the nonlinearities are more and more obvious after the model joins the transient voltage stabilization constraints, and the DE is caught in the local optimum, while DDPG adopts a deterministic strategy, which can quickly converge to the target value and also does not fall into local optimum.

Table 4. The number and time of iterations of different calculation methods

Calculation method of PSC	Number of calculations	TSC/MW
DDPG	3820	9348
DE	5925	8824

4.5.3. Comparison with other reinforcement learning algorithms. In order to verify the efficiency of DDPG algorithm on TSC computation, it is compared with Q-learning (QL) [27], flexible strategy-evaluation (SAC) [28] and proximal policy optimization algorithm (PPO) [29]. The curves of the loss functions of the different algorithms with respect to the number of training times are shown in Fig. 14. The comparison results of the number of training times and training time are shown in Fig. 15, respectively.

From Fig. 14 and Fig. 15, it can be seen that:

1) The loss function of the DDPG algorithm converges the fastest, converging to 0 loss in about 3200 times, while the other three algorithms all begin to converge to 0 after 4000 times of training, which is poor convergence, and the DDPG has the least number of training times and the shortest training time, which is computationally efficient.

2) QL has the longest number of training times and training time because QL has discrete actions in training and QL uses Q-tables for storing Q-values and state actions, whereas DDPG has continuous actions and uses a neural network to make the input state actions and output Q-values into a function, which is fitted by training, and the learning is more stable and easier to converge.

3) SAC has relatively more training times and training time because SAC uses a random strategy in the training process, which requires more training times and time, whereas DDPG uses a deterministic strategy, which can quickly converge to the target value.

4) PPO has the slowest convergence because PPO uses on-policy which has the problem of invalid samples, while DDPG uses off-policy which utilizes samples effectively and improves the training efficiency.

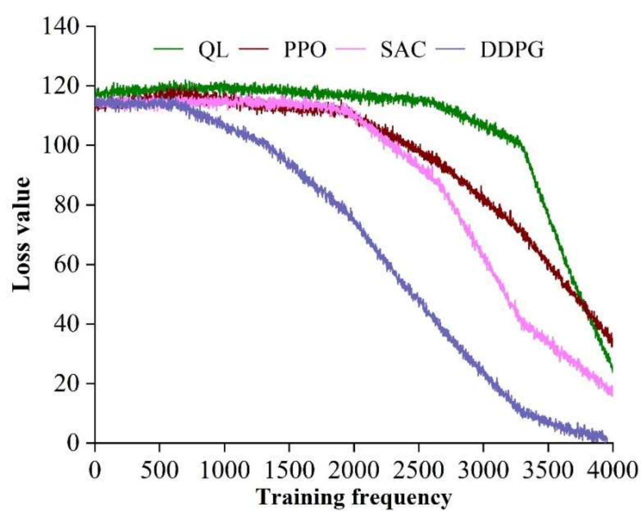

Fig. 14. Loss function curves of different algorithms with training times

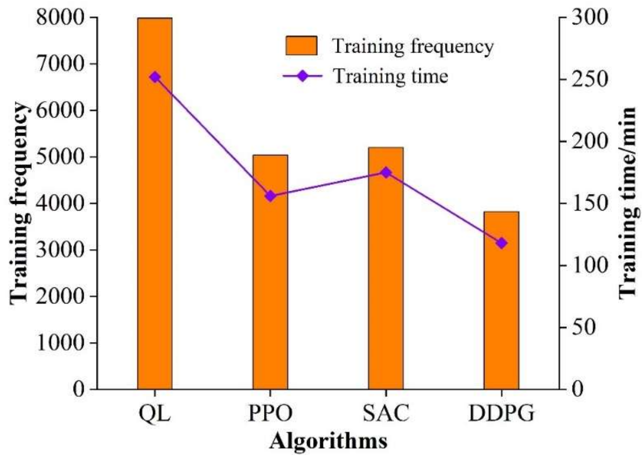

Fig. 15. Training frequency and time of different algorithms

In summary, after the introduction of transient voltage stabilization constraints, the nonlinear characteristics of the model in this paper are more obvious, and conventional TSC calculation methods such as DE are easy to fall into local optimal solutions. Compared with other reinforcement learning algorithms, the DDPG algorithm uses continuous action to search for TSC in the interaction between the intelligent body and the environment, which improves the efficiency and accuracy of the computation, and at the same time adopts a deterministic strategy and utilizes neural network learning to improve the training stability.

5. Conclusion

In this paper, we investigate the TSC calculation problem of power grids in multi-temporal scales by constructing a TSC model of dynamically partitioned flexible interconnected grids and solving the model using the DDPG algorithm.

In the TSC obtained by the stepwise approximation method without considering the transient voltage stabilization constraints and the DDPG algorithm, the time periods in which the voltage at node 54 is less than 0.80 p.u. are 0.31-3.72 s and 0.31-7.05 s, respectively, both of which are greater than 1.0 s, and the transient voltage is destabilized. While the DDPG algorithm considering the transient voltage stabilization constraints, the obtained node 54 voltage is greater than 0.80 p.u. Therefore, the transient voltage stabilization constraints of the TSC model in this paper can effectively reduce the risk of transient voltage destabilization of the power grid. On the other hand, the TSC of the grid is significantly improved with the increase of the capacity of the zonal flexible interconnectors, and the TSC is reduced by the dynamic voltage stabilization constraints under the same capacity. However, when the capacity exceeds 900 MW, the TSC increase is not obvious, the configuration cost is higher, and the TSC decreases to a lesser extent affecting the economy, which indicates the reasonableness of the device capacity setting in this paper.

In open-loop operation, the TSCs of A and B are 4366 MW and 4330 MW, respectively, and the sum of the TSCs of the two zones is 8696 MW, while the sum of the TSCs of the two zones is 9348 MW after the zonal flexible interconnection, which indicates that, compared with the open-loop operation of the zones, the zonal flexible interconnection adopted in this paper's experimental grid is able to effectively improve the overall TSC level of the grid.

In addition, compared with the traditional TSC calculation method - DE algorithm, the DDPG algorithm used in this paper has relatively fewer calculations (3820 times < 5925 times) and the calculated TSC is relatively larger (9348MW > 8824MW). And comparing with reinforcement learning algorithms such as QL, SAC and PPO, DDPG algorithm has higher computational efficiency and accuracy.

Funding

This research was supported by the State Grid Headquarters Project: Key Technologies and Applications for Supply-Demand Risk Identification and Planning Decision Simulation of Provincial Power Grids with High Penetration of Renewable Energy (1400-202324646A-3-2-ZN).

References

[1] Xu, Z., Das, D. K., Guo, W., & Wei, W. (2021). Does power grid infrastructure stimulate regional economic growth?. Energy Policy, 155, 112296.

[2] Radley, B., & Lehmann-Grube, P. (2022). Off-grid solar expansion and economic development in the global South: A critical review and research agenda. Energy Research & Social Science, 89, 102673.

[3] Bigerna, S., Bollino, C. A., & Micheli, S. (2016). Socio-economic acceptability for smart grid development–a comprehensive review. Journal of Cleaner Production, 131, 399-409.

[4] Yang, F., Zhang, S., & Sun, C. (2020). Energy infrastructure investment and regional inequality: Evidence from China's power grid. Science of the Total Environment, 749, 142384.

[5] Eicke, A., Ruhnau, O., & Hirth, L. (2021). Electricity balancing as a market equilibrium: An instrument-based estimation of supply and demand for imbalance energy. Energy Economics, 102, 105455.

[6] Gan, L., Jiang, P., Lev, B., & Zhou, X. (2020). Balancing of supply and demand of renewable energy power system: A review and bibliometric analysis. Sustainable Futures, 2, 100013.

[7] Rao, H., Han, F., Chen, Z., Huang, G., Wang, D., Zhang, Y., ... & Zhou, B. (2023). Strategy for guaranteeing power supply security of China. Strategic Study of Chinese Academy of Engineering, 25(2), 100-110.

[8] Romanova, V., Khromov, S., & Suslov, K. (2023, January). Ensuring the reliability of power supply systems by improving the quality of electrical energy. In AIP Conference Proceedings (Vol. 2552, No. 1). AIP Publishing.

[9] Xu, Z., Li, J., Liu, H., Ge, S., Wang, B., & Wen, Z. (2024). Reliability-based power supply capability evaluation of power distribution networks considering interruptible loads after contingencies. Sustainable Energy Technologies and Assessments, 69, 103876.

[10] Belyaev, N., Egorov, A., Korovkin, N., & Chudny, V. (2018). Economic aspects of ensuring the capacity adequacy of electric power systems. In E3S Web of Conferences (Vol. 58, p. 01010). EDP Sciences.

[11] Mahmood, H., Wen, J., Zakaria, M., & Khalid, S. (2022). Linking electricity demand and economic growth in China: evidence from wavelet analysis. Environmental Science and Pollution Research, 29(26), 39473-39485.

[12] Akpeji, K. O., Olasoji, A. O., Gaunt, C. T., Oyedokun, D. T., Awodele, K. O., & Folly, K. A. (2020). Economic impact of electricity supply interruptions in South Africa. SAIEE Africa Research Journal, 111(2), 73-87.

[13] Hussain, S., Xuetong, W., & Maqbool, R. (2023). Understanding the power disruption and its impact on community development: An empirical case of Pakistan. Sustainable Energy Technologies and Assessments, 55, 102922.

[14] Qiu, Y., Deng, N., Wang, B., Shen, X., Wang, Z., Hultman, N., ... & Wang, Y. D. (2024). Power supply disruptions deter electric vehicle adoption in cities in China. Nature Communications, 15(1), 6041.

[15] Biryulin, V. I., Kudelina, D. V., & Larin, O. M. (2020, May). Electricity quality problems in the 0.4 kV city electric networks. In 2020 International Conference on Industrial Engineering, Applications and Manufacturing (ICIEAM) (pp. 1-6). IEEE.

[16] Meng, Q., Tong, X., Hussain, S., Luo, F., Zhou, F., He, Y., ... & Li, B. (2024). Enhancing distribution system

stability and efficiency through multi‐power supply startup optimization for new energy integration. IET Generation, Transmission & Distribution, 18(21), 3487-3500.

[17] Popov, M. G., Bazlov, D. A., & Tarasevich, M. D. (2020, January). High-speed automation for ensuring the stability of a small-power system. In 2020 IEEE Conference of Russian Young Researchers in Electrical and Electronic Engineering (EIConRus) (pp. 824-829). IEEE.

[18] Braun, L., Le, M., Motz, J., & Birke, K. P. (2022). Novel Approach to Ensure Safe Power Supply for Safety-Relevant Consumers. Batteries, 8(5), 47.

[19] Yi, Z. H. A. N. G., Feng, Z. H. A. N. G., Youchun, L. I., Lv, T. A. N. G., Xuehu, P. E. N. G., & Jianguo, M. O. (2021, February). Analysis Of Typical Power Grid Blackout Accidents And Suggestions For Countermeasures. In Journal of Physics: Conference Series (Vol. 1754, No. 1, p. 012023). IOP Publishing.

[20] Ferreira, E. F., & Barros, J. D. (2018). Faults monitoring system in the electric power grid of medium voltage. Procedia computer science, 130, 696-703.

[21] Rivas, A. E. L., & Abrao, T. (2020). Faults in smart grid systems: Monitoring, detection and classification. Electric Power Systems Research, 189, 106602.

[22] Triki-Lahiani, A., Abdelghani, A. B. B., & Slama-Belkhodja, I. (2018). Fault detection and monitoring systems for photovoltaic installations: A review. Renewable and Sustainable Energy Reviews, 82, 2680-2692.

[23] Przystupa, K. (2018). Selected methods for improving power reliability. Przegląd Elektrotechniczny, 94(12), 270-273.

[24] Yi Zhu, Zexin Li, Jinyong Wang, Ying Zhao & Miaoer Li. (2025). Behavior Safety Decision-Making Based on Deep Deterministic Policy Gradient and Its Verification Method. Symmetry(1),132-132.

[25] AnasNawfel Saidi & MohamedLehsaini. (2025). A Deep Q‐Learning Approach for an Efficient Resource Management in Vehicle‐to‐Everything Slicing Environment. International Journal of Communication Systems(4),e6137-e6137.

[26] Chinmay Saha, Dipak Kumar Jana & Avijit Duary. (2024). Erratum to "Enhancing production inventory management for imperfect items using fuzzy optimization strategies and Differential Evolution (DE) algorithms" . Franklin Open100123-100123.

[27] Sreyas Ramesh, Sukanth B N, Sri Jaswanth Sathyavarapu, Vishwash Sharma, Nippun Kumaar A. A. & Manju Khanna. (2025). Comparative analysis of Q-learning, SARSA, and deep Q-network for microgrid energy management. Scientific Reports(1),694-694.

[28] Linfei Yin & Wenxuan Huang. (2025). Informer-embedded prioritized experience replay-based soft actor-critic for ultra-low frequency oscillation suppression of pumped hydropower storage systems. Journal of Energy Storage(PA),115802-115802.

[29] Yuchen Wang, Ruxin Xiao, Xinheng Wang & Junqing Zhang. (2025). Viewpoint planning optimization for structure from motion-based 3D reconstruction of industrial products with sim-to-real proximal policy optimization. Expert Systems With Applications126674-126674.